25th ABCM International Congress of Mechanical Engineering
October 20-25, 2019, Uberlândia, MG, Brazil

COBEM2019-1069
NUMERICAL SIMULATIONS OF UNSTEADY-FLOWS OF HERSCHEL-BULKLEY FLUID IN A TAYLOR-COUETTE GEOMETRY

Felipe R. Loyola
Waldyr L. Silva Jr.
Department of Mechanical Engineering, Federal University of Paraná, 81531990 Curitiba, PR, Brazil
felipeloyola@gmail.com
waldyr@ufpr.br

Abstract. *In the present work, the periodic flow pattern of a top-load vertical axis washing machine is numerically modeled as the so-called Taylor-Couette flow by means of the mass and momentum transport from an agitator to the fluid stream. The characterization procedure of the fabric-water mixtures fluid flow, within the washing machine, as a Herschel-Bulkley fluid model demonstrated that is capable to reproduce such a complex flow behavior with a satisfactory degree of reliability. Moreover, the fabric dispersal and deformation on water according to the applied shear stress from the spin bowl may be seen as the change of the apparent viscosity in the physical domain. Therefore, the computed rheological behavior of different fabric-water mixtures from periodic simulations, which attempts to simulate a complete cycle of a real washing machine agitation profile, were analyzed. The rheological mixtures characterization was obtained from previous work. Higher values of the apparent viscosity were observed in regions near the agitator and the bottom surface, thus pointing out where the efforts to enhance the mechanical washing efficiency should be addressed.*

Keywords: *Rheology, Herschel-Bulkley Model, Periodic Flows, Numerical Simulations*

1. INTRODUCTION

A top-load washing machine, which the main purpose is to remove dirt from a given amount of fabric by means of mechanical, thermal, and chemical processes (Van den Brekel, 1987), may be simplified as a structure of concentric cylinders where the inner cylinder (agitator), which is responsible for moving the fabric-water mixture, rotates with controlled torque and angular velocity and the outer cylinder remains stationary. In general, the washing process depends on a wide set of parameters, such as the spin bowl and agitator geometries, the agitation profile (i.e., temporal variation of torque, angular swept and speed), the water level, and the temperature of the mixture formed by water, fabric, detergent, among other additives (Campos and Hermes 2016). It is worth mentioning the efficiency of the mechanical washing process relies on the mass and momentum transport from the agitator to the fluid stream, characterizing a periodic circular flow (Loyola et al, 2018). Still, a satisfactory level of understanding of the mechanical process can be obtained from the so-called Taylor-Couette flow whose main characteristic is the confinement of a viscous fluid between two rotating cylinders (Donnelly 1991).

In a physical model for a typical Taylor-Couette flow, the fluid column height is denoted by h, whereas the cylinders total height is denoted by H, as illustrated in Figure 1. One can see that Figure 1 (b) represents a vertical cut of the physical domain, denoting only a slice from the r-z axis only in any angular position. For the sake of simplicity, the outer cylinder (drum) is held stationary while the inner one (agitator) rotates independently with an imposed angular velocity ω_{inn}. The radius gap ($\delta = R_{out} - R_{inn}$), radius ratio ($k = R_{inn}/R_{out}$) and aspect ratio ($\Gamma = h/\delta$) are the geometric parameters. The dimensionless flow parameters are the rotational Reynolds number ($Re = \rho(\omega R_{inn})\delta/\mu$) and Taylor number ($Ta = (k^{-1}-1)Re^2$), the former is the ratio between inertial and viscous forces acting on the flow, whereas the latter relates the same forces taking the cylindrical geometry into account.

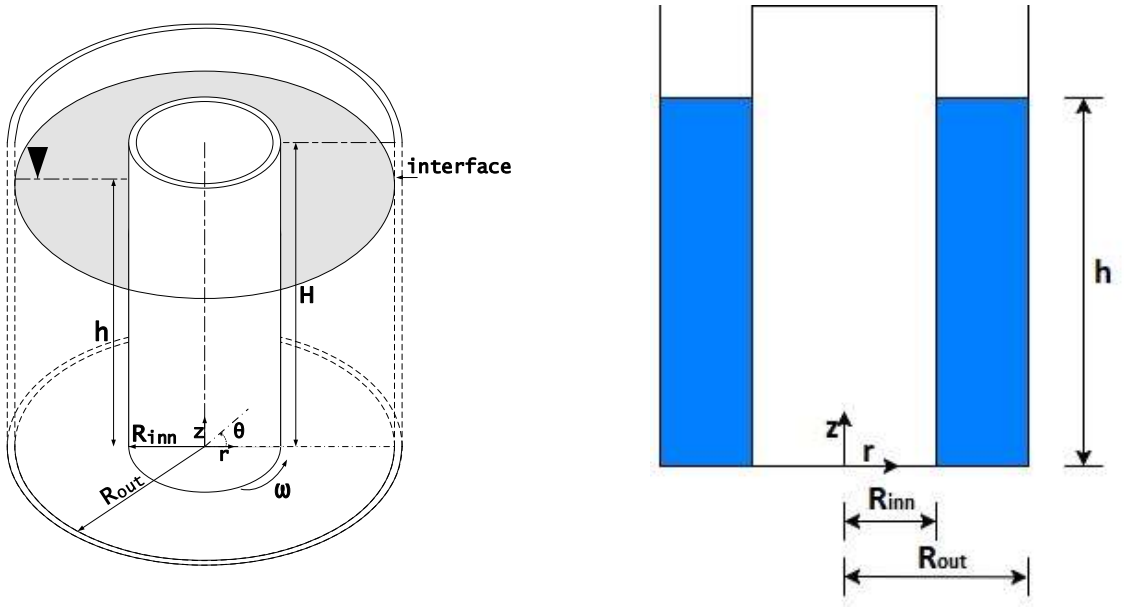

(a) (b)

Figure 1. (a) Physical domain of the Taylor-Couette flow; (b) vertical cut of the physical domain

The angular velocity profile of the inner cylinder over time is illustrated in Figure 2. Firstly, an abrupt acceleration takes place, later the cylinder maintains the maximum velocity for a short period of time. So, the velocity decreases until the cylinder stops (i.e., time off). The same operation is repeated in the opposite direction.

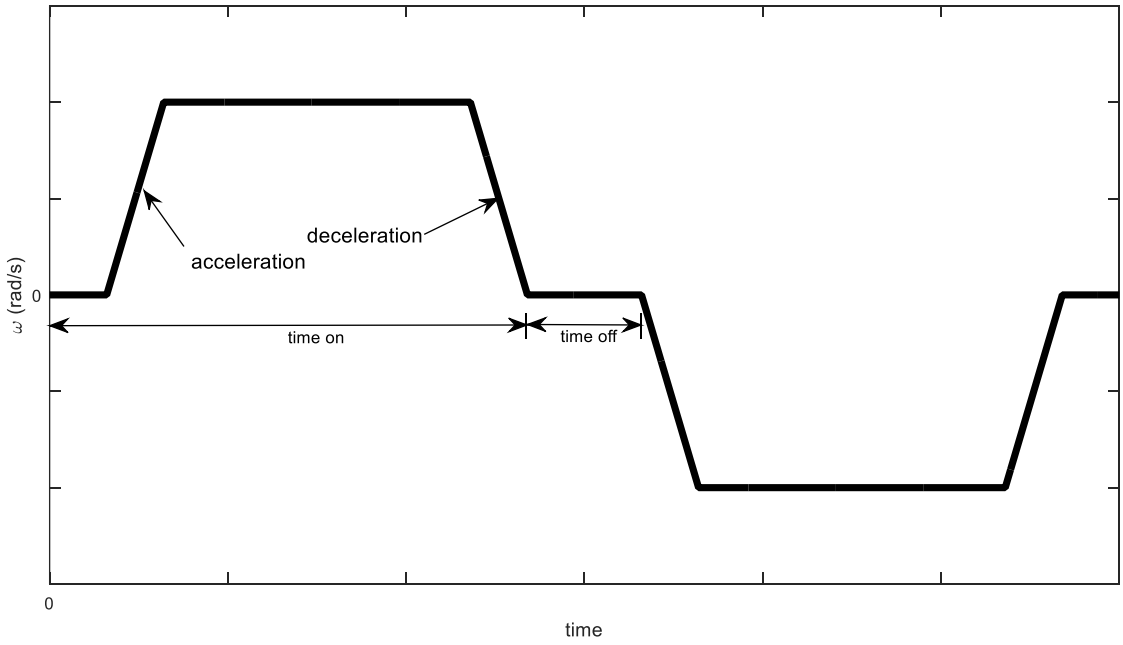

Figure 2. Angular velocity profile

2. MATHEMATICAL FORMULATION

Given the second-order partial differential momentum transport equations, with advective-diffusive nature, two boundary conditions in each direction (θ, r, and z) are required. The mass and momentum conservation equations (in their conservative forms), in all three cylindrical directions (tangential, radial, and axial), are respectively as follows:

$$\frac{\partial \rho}{\partial t}+\frac{1}{r}\frac{\partial(\rho r v_r)}{\partial r}+\frac{1}{r}\frac{\partial(\rho v_\theta)}{\partial \theta}+\frac{\partial(\rho v_z)}{\partial z}=0 \tag{1}$$

$$\frac{\partial(\rho v_\theta)}{\partial t}+\frac{\partial(\rho v_r v_\theta)}{\partial r}+\frac{1}{r}\frac{\partial(\rho v_\theta v_\theta)}{\partial \theta}+\frac{\rho v_r v_\theta}{r}+\frac{\partial(\rho v_z v_\theta)}{\partial z}=\mu\left[\frac{1}{r^2}\frac{\partial^2 v_\theta}{\partial \theta^2}+\frac{\partial}{\partial r}\left(\frac{1}{r}\frac{\partial}{\partial r}(r v_\theta)\right)+\frac{\partial^2 v_\theta}{\partial z^2}+\frac{2}{r^2}\frac{\partial v_r}{\partial \theta}\right]-\frac{1}{r}\frac{\partial p}{\partial \theta}+\rho g_\theta \tag{2}$$

$$\frac{\partial(\rho v_r)}{\partial t}+\frac{\partial(\rho v_r v_r)}{\partial r}+\frac{1}{r}\frac{\partial(\rho v_\theta v_r)}{\partial \theta}-\frac{\rho v_\theta^2}{r}+\frac{\partial(\rho v_z v_r)}{\partial z}=\mu\left[\frac{1}{r^2}\frac{\partial^2 v_r}{\partial \theta^2}+\frac{\partial}{\partial r}\left(\frac{1}{r}\frac{\partial}{\partial r}(r v_r)\right)+\frac{\partial^2 v_r}{\partial z^2}-\frac{2}{r^2}\frac{\partial v_\theta}{\partial \theta}\right]-\frac{\partial p}{\partial r}+\rho g_r \tag{3}$$

$$\frac{\partial(\rho v_z)}{\partial t}+\frac{\partial(\rho v_r v_z)}{\partial r}+\frac{1}{r}\frac{\partial(\rho v_\theta v_z)}{\partial \theta}+\frac{\partial(\rho v_z v_z)}{\partial z}=\mu\left[\frac{1}{r^2}\frac{\partial^2 v_z}{\partial \theta^2}+\frac{1}{r}\frac{\partial}{\partial r}\left(r\frac{\partial v_z}{\partial r}\right)+\frac{\partial^2 v_z}{\partial z^2}\right]-\frac{\partial p}{\partial z}+\rho g_z \tag{4}$$

where the gravitational force is acting only in the axial direction (z). The set of equations is composed by four variables (v_θ, v_r, v_z, and P) [m/s, and Pa] and three momentum equations, which must be coupled with the mass conservation one to obtain the pressure field of the flow. For a Taylor-Couette geometry, the boundary conditions are as follows:

- At $z = 0 \rightarrow (v_\theta , v_r , v_z) = (0 , 0 , 0)$ for $R_{inn} \leq r \leq R_{out}$, (bottom)base surface;
- At $z = H \rightarrow (\partial v_\theta/\partial z , \partial v_r/\partial z , v_z) = (0 , 0 , 0)$ for $R_{inn} \leq r \leq R_{out}$, open surface;
- For $r < R_{inn} \rightarrow (v_\theta , v_r , v_z) = (0 , 0 , 0)$ for $0 \leq z \leq H$, inside the inner cylinder;
- At $r = R_{inn} \rightarrow (v_\theta , v_r , v_z) = (\omega R_{inn} , 0 , 0)$ for $0 \leq z \leq H$; inner cylinder rotation;
- At $r = R_{out} \rightarrow (v_\theta , v_r , v_z) = (0 , 0 , 0)$ para $0 \leq z \leq H$; static outer cylinder;
- Neumann boundary condition is applied for the pressure field on all the surfaces;
- Cyclic boundary condition for $\theta = 0$ and $\theta = 2\pi$

In this particular study, the fluid flow is considered as isothermal, incompressible and laminar, without natural convection and viscous heating, so that the apparent viscosity (η) [Pa·s] depends only on the second invariant of the strain-rate tensor ($\bar{\bar{\dot{\gamma}}}$) [s^{-1}]. Therefore, the rheological behaviors, based on the Herschel-Bulkley model, obtained through experimental data reduction by Loyola et al (2018) are applied in order to simulate the fluid flow of the fabric-water within concentric cylinders, and their parameters for different fabric-water suspensions, consisted of mass-balanced mixture of 400 cm² (20 x 20 cm) cotton and semi-synthetic fabrics, are depicted in Table 1, where one can note that all the fluids present a shear-thickening behavior (flow behavior index above the unity).

The experimental apparatus used by Loyola et al (2018) consisted of a double concentric cylinder structure, with a rotating plastic inner cylinder of 73 mm radius (R_{inn}) and a stationary aluminum-made drum – outer cylinder, with 269 mm radius (R_{out}), which is considered a wide-gap geometry ($k = R_{inn}/R_{out} \approx 0.4$). All the tests were carried out with 64 L of fluid (fabric-water mixture), which is a fluid column of 316mm height (axial direction).

Table 1. Rheological behavior of different fabric-water mixtures obtained by Loyola et al (2018)

Name	Fabric	Fabric mass	Rheological Behavior
Mix 1	Mixed	1.25	$\bar{\bar{\tau}} = \left(2.28\lvert\dot{\gamma}\rvert^{1.27-1} + \frac{0.75}{\lvert\dot{\gamma}\rvert}\right)\bar{\bar{\dot{\gamma}}}$
Mix 2	Mixed	2.50	$\bar{\bar{\tau}} = \left(3.77\lvert\dot{\gamma}\rvert^{1.25-1} + \frac{1.23}{\lvert\dot{\gamma}\rvert}\right)\bar{\bar{\dot{\gamma}}}$

3. NUMERICAL SCHEME

In order to solve the simulation of fabric-water mixture flows within two concentric cylinders by means of a homemade three-dimensional finite-volume model, based on the mass and momentum conservation equations, written in cylindrical coordinates (Equations 1 to 4), the following methodologies have been applied:

- Velocity-pressure coupling by the PRIME method (Maliska and Raithby 1983);
- Staggered grid for the velocities control volumes;
- Collocated grid for the pressure field (Patankar 1980);
- A non-uniform cylindrical grid at r and z-axes;
- Power-Law interpolation scheme (Patankar 1980);
- Biconjugate gradient stabilized method (BiCGSTAB) to solve the linear system (Van der Vorst 1992);
- TDMA (Tridiagonal Matrix Algorithm) as the preconditioner for the BiCGSTAB method. The line-by-line method is applied for the radial and axial axes, while on θ axis, due to its cyclic boundary condition, the CTDMA (Cyclic Tridiagonal Matrix Algorithm) method is used (Ahlberg et al 1967);
- No-slip (Dirichlet-type) boundary conditions applied when the surface velocity is zero; Neumann-type boundary conditions applied to the pressure field in all directions

For a Hershel-Bulkey fluid model, which combines the effects of the Power-Law and the Bingham models, there is no flow when the applied shear stress is smaller than the yield stress, thus producing two different regions, the unyielded and the flow region. In order to avoid discontinuities, which may lead to numerical convergence issues, Papanastasiou (1987) proposed a modification in the accounted apparent viscosity for yield fluid models by smoothing the discontinuity by means of a parameter K, which controls the exponential growth of the shear stress (Mitsoulis, 2007). Therefore, this modification when applied to the Hershel-Bulkley model yields to:

$$\bar{\bar{\tau}} = \left(m|\dot{\gamma}|^{n-1} + \frac{\tau_0}{|\dot{\gamma}|}[1-\exp(-K|\dot{\gamma}|)] \right) \bar{\bar{\dot{\gamma}}} \tag{5}$$

For the transient simulations, a mesh grid with 50, 65 and 50 points in tangential (θ), radial (r) and axial (z) directions, respectively, was implemented. Hence, the three-dimensional cylindrical mesh presents a total of 162,500 nodal points to represent the entire discretized physical domain (R_{inn} = 110 mm, R_{out} = 269 mm, and H = 316 mm). Plots of the shear rate ($\dot{\gamma}_{\theta\theta}$, $\dot{\gamma}_{rr}$, $\dot{\gamma}_{zz}$, $\dot{\gamma}_{r\theta}$, $\dot{\gamma}_{\theta z}$, and $\dot{\gamma}_{rz}$) components and velocities components (v_θ, v_r, and v_z), as well as shear stress components and shear stress tensor modulus, pressure, residues, and stream function distributions, were computed at each time-step to evaluate the flow evolution in time.

Torque values were used as the comparison parameter between the simulation results and the experimental data. Considering that the aspect ratio in this work is not high enough to neglect the end effects ($\Gamma \approx 2$) and the water-fabric mixture is not uniform, the numerical computation of the torque on the inner cylinder surface was calculated by the following relation:

$$T = \int_0^{2\pi} \int_0^{H} |\tau| R_{inn} dz d\theta \tag{6}$$

In the present work, both mass and momentum convergence are monitored to advance the simulation to the next time step. If both mass and momentum conservation residues, for all the control volumes, converge to a value below the tolerance, the simulation proceeds to the next time step.

4. RESULTS

In the periodic flow simulations, only the two bulks of mixed fabric-water suspensions were used as the working fluid (Table 1). In this context, for the purpose of comparing the torque values over time (Figure 3), only the cases where the base is maintained at rest is evaluated. A time-step (Δt) of 80 milliseconds was applied for all the simulations. Four different test simulations were carried out concerning periodic conditions, which attempts to approximate the operation conditions of a real vertical-axis washing machine. All the simulation conditions have swift acceleration and deceleration steps, where the difference between them is the maximum velocity. Tests 1 and 2 have the following cycling characteristics: acceleration and deceleration times of 0.32 s each, time in the constant maximum velocity of 1.72 s, and time-off of 0.64 s. The maximum velocity is of 40 rpm in Test 1, and 80 rpm in Test 2. Tests 1 and 2 complete cycles (clockwise and counterclockwise directions) last for six seconds, while Tests 3 and 4 last for three seconds. The verification of the computed torque on inner cylinder surface compared to the experimental measurement was presented on the work of Loyola et al (2018), where the numerical responses for all tests are in good agreement with experimental measurements, despite not being able to represent the torque peaks observed in the experimental results. Figure 3 depicts the numerically computed torque in the whole inner cylinder surface over time. Figure 3 (a) shows the torque for Tests 1

and 2, while (b) shows the torque for Tests 3 and 4. One can see the difference between the presented torque value for the different mixtures at the time-on period, while that at time-off period the torque values tend to zero for all tests. Despite the fact that the inner cylinder rotates in clockwise and counterclockwise directions, all the numerical torque values presented are positive.

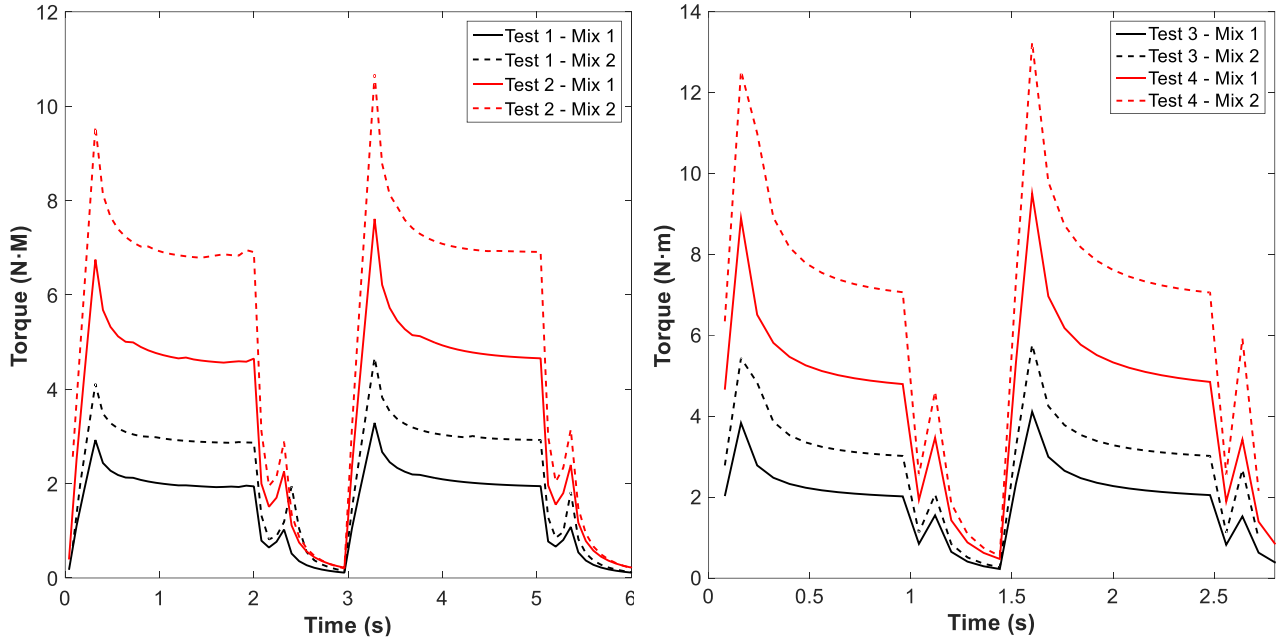

(a) (b)

Figure 3. Numerical computed torque values for: (a) Tests 1 and 2; (b) Tests 3 and 4

4.1 Presence of the rotating bottom basis

Figure 4 depicts the apparent viscosity (η) field at different times of Test 2 for the water-fabric mixture with 1.25 kg case (Mix 1). The first column points out the time of 2.0 s when the last instant with the maximum counterclockwise velocity (80 rpm), the second column points out the time of 2.96 s at the end of the time-off period, and finally the last column points out the time of 5.04 s, which is the last instant with the maximum clockwise velocity of the inner cylinder.

Figure 4 (a), (b), and (c) depicts the vertical field of the apparent viscosity at $\theta = 90°$ at the different time instants. One can see that due to the shear thickening characteristic of the mixture, the area with the maximum applied shear stress presents the higher apparent viscosity. Moreover, the apparent viscosity also changes along the z-axis, presenting a smaller viscosity at the top because of the open-boundary condition and milder shear stress applied into the mixture. The apparent viscosities are very similar for the time instants with maximum velocity, despite the flow direction, and presents smaller values at the end of time-off period when there is no shear stress applied into the flow.

Figure 1 (d), (e), and (f) depicts a polar radial view of the apparent viscosity field at the height corresponding to 10% of the maximum height. A quiver field is also presented to illustrate the velocity direction and intensity along with the tangential and radial directions. One can see the differences in the apparent viscosity observed in the vertical fields also observed in the polar radial view, where the higher apparent viscosity values are observed at the height near the bottom base and near the inner cylinder wall because of the imposed shear stress into the fluid. The tighter viscosity contrast, without applied shear stress, at the time-off period, is observed as well. Figure 1 (g), (h), and (i) presents the polar radial view at the half-height position, and (j),(k), and (l) at approximately 90% of the maximum height, where one can see that the polar view corresponds to the vertical axis illustration (a, b, c). The apparent viscosity field is weaker near the top position because of the open boundary condition.

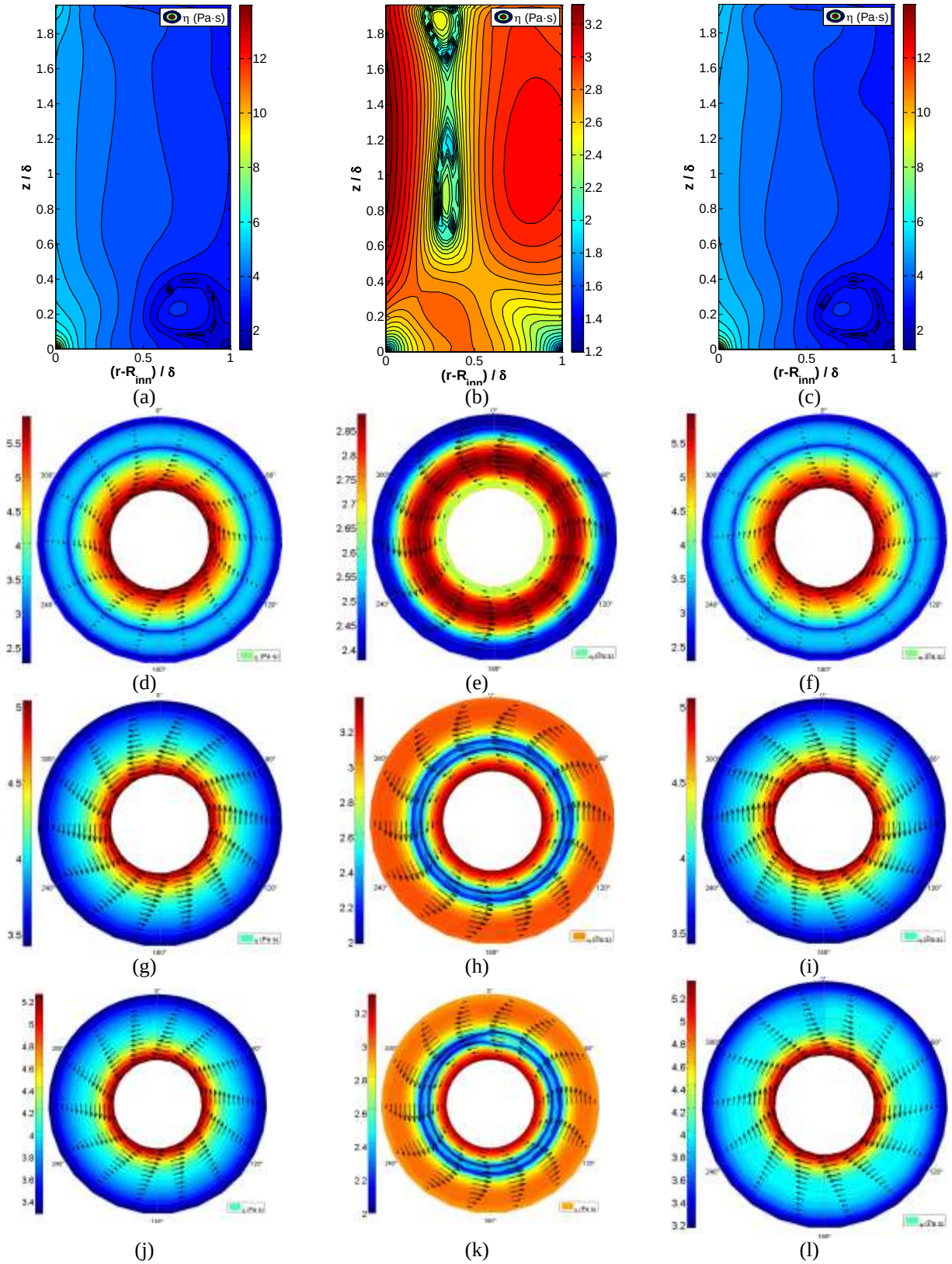

Figure 4. Apparent viscosity fields observed in different positions and at different time instants of the periodic simulations (Test 2) without the rotating basis: (a,b, c) vertical field; (d, e, f) polar view at 10% of the maximum height; (g, h, i) polar view at the half-height position; and (j, k, l) polar view at the 90% of the maximum height position.

Similarly, the same analysis is made for the case where the bottom basis is rotated with the inner cylinder in Figure 5 and its respective subindexes. In this case, one can see that the maximum torque is computed at the outer point of the bottom basis, and its values are higher than for the case where the bottom basis is static because of the maximum tangential

velocity value. The presence of a rotating basis enhances the flow intensity over time along with the velocity profile, which favors the fluid mixing within the cylinders.

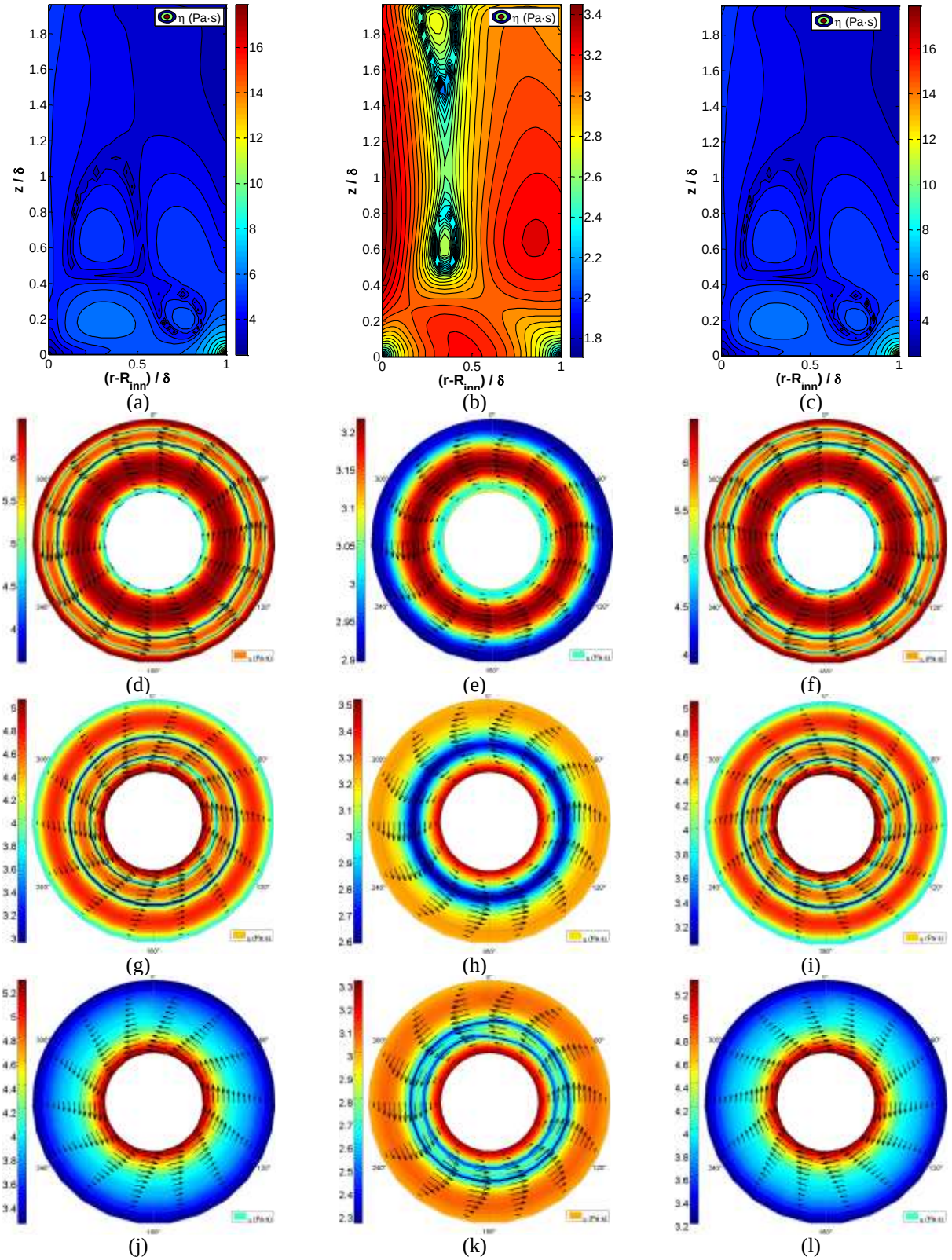

Figure 5. Apparent viscosity fields observed in different positions and at different time instants of the periodic simulations (Test 2) with the rotating basis: (a,b, c) vertical field; (d, e, f) polar view at 10% of the maximum height; (g, h, i) polar view at the half-height position; and (j, k, l) polar view at the 90% of the maximum height position.

4.2 Different Mixtures

Figure 6 illustrates the apparent viscosity field at different times for both the fabric-water mixtures (Mix 1 and Mix 2) for the computed results of test 4. Figure 6 (a) depicts the apparent viscosity field at 1.0 seconds, which is the last instant with the maximum velocity in the time-on period, while (b) depicts the field at 1.48 seconds (the last instant of the time-off period), and (c) represents the field at 2.52 seconds, which is the last instant of the inner cylinder with the maximum velocity in the counterclockwise direction. Similarly, Figure 6 (d), (e), and (f) depicts the apparent viscosity field at the same time instants for the simulations using the Mix 2 as the working fluid. One can see that the fields are qualitatively similar in all the time instants for both fluids, where only minor differences are observed because of the different behavior index (n) for the fluids. The major difference comes from the maximum values observed due to the different flow consistency index (m) and the yield shear stress (τ_0) for both fluids.

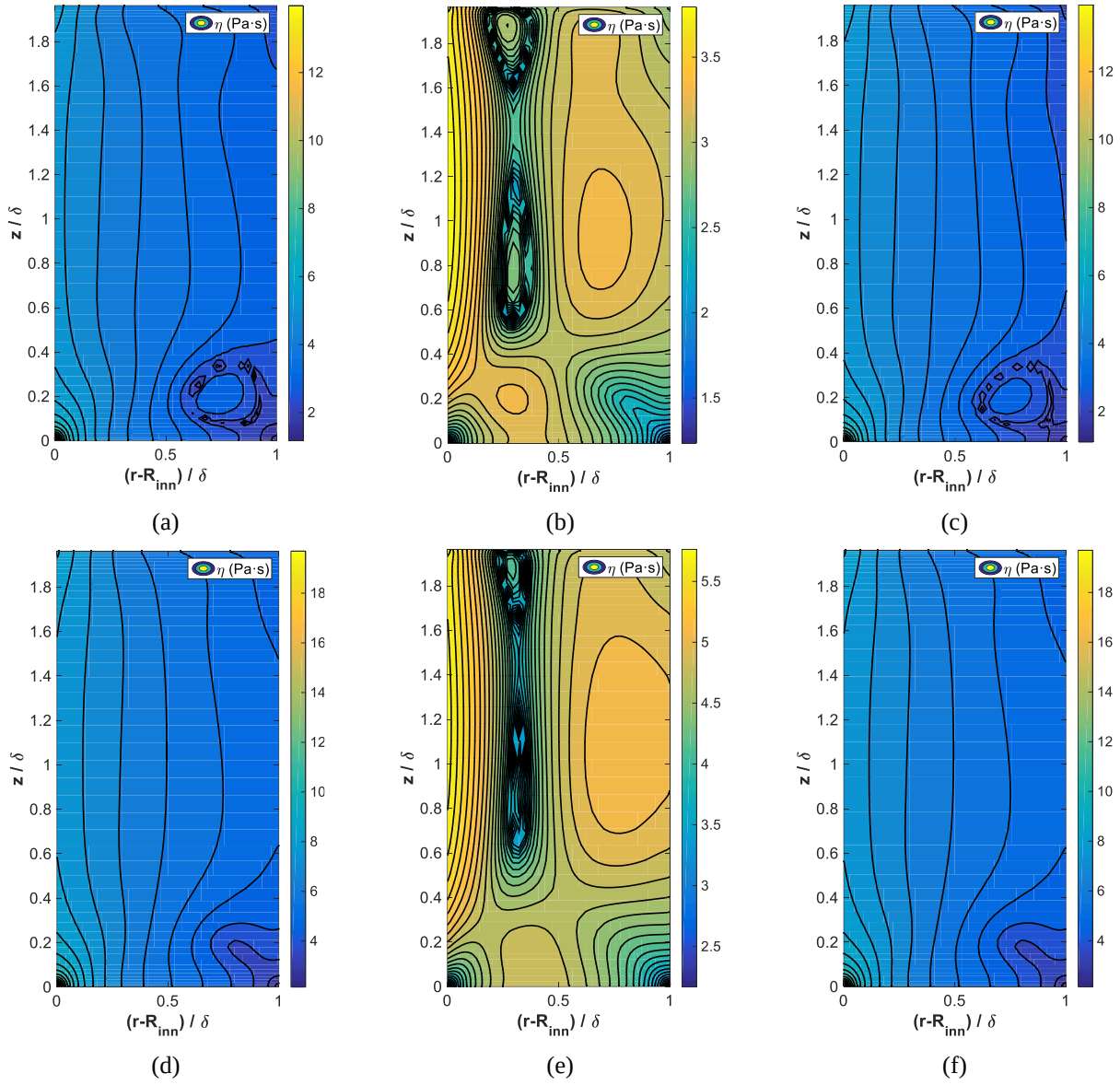

Figure 6. Apparent viscosity fields observed in different positions and at different time instants of the periodic simulations for Test 4: for Mix 1 (a) 1.0 s; (b) 1.48 s; (c) 2.52 s, and for Mix 2 (d) 1.0 s; (e) 1.48 s; (f) 2.52.

4.3 Different Tests

Finally, the last comparison is presented concerning the simulations for Mix 2, without the rotating basis for the four different tests. All the pair of figures illustrates the last instant of the time-on period and the time-off period, which is 2.0 and 2.96 seconds for Tests 1 and 2, and 1.0 and 1.48 second for Tests 3 and 4. Figure 7 (a) and (b) depicts the apparent viscosity fields for Test 1, (c) and (d) Test 2, (e) and (f) Test 3 and (g) and (h) Test 4. The major difference comes from

the maximum viscosity values observed for Tests 2 and 4, in comparison with Tests 1 and 3, while minor differences are observed at the apparent viscosity field distribution in the different tests. One may note that small differences of the maximum viscosity are observed between Tests 1 and 3, and Tests 2 and 4, which is different from the behavior pointed out in Figure 3, as the shear stress and the torque values are directly related. However, the main differences come right after the acceleration and deceleration period, which is pointed out by means the torque peaks in Figure 3. After the time-on period, the flow behavior tends to be the same for the different tests, despite the short time-on periods for Tests 3 and 4.

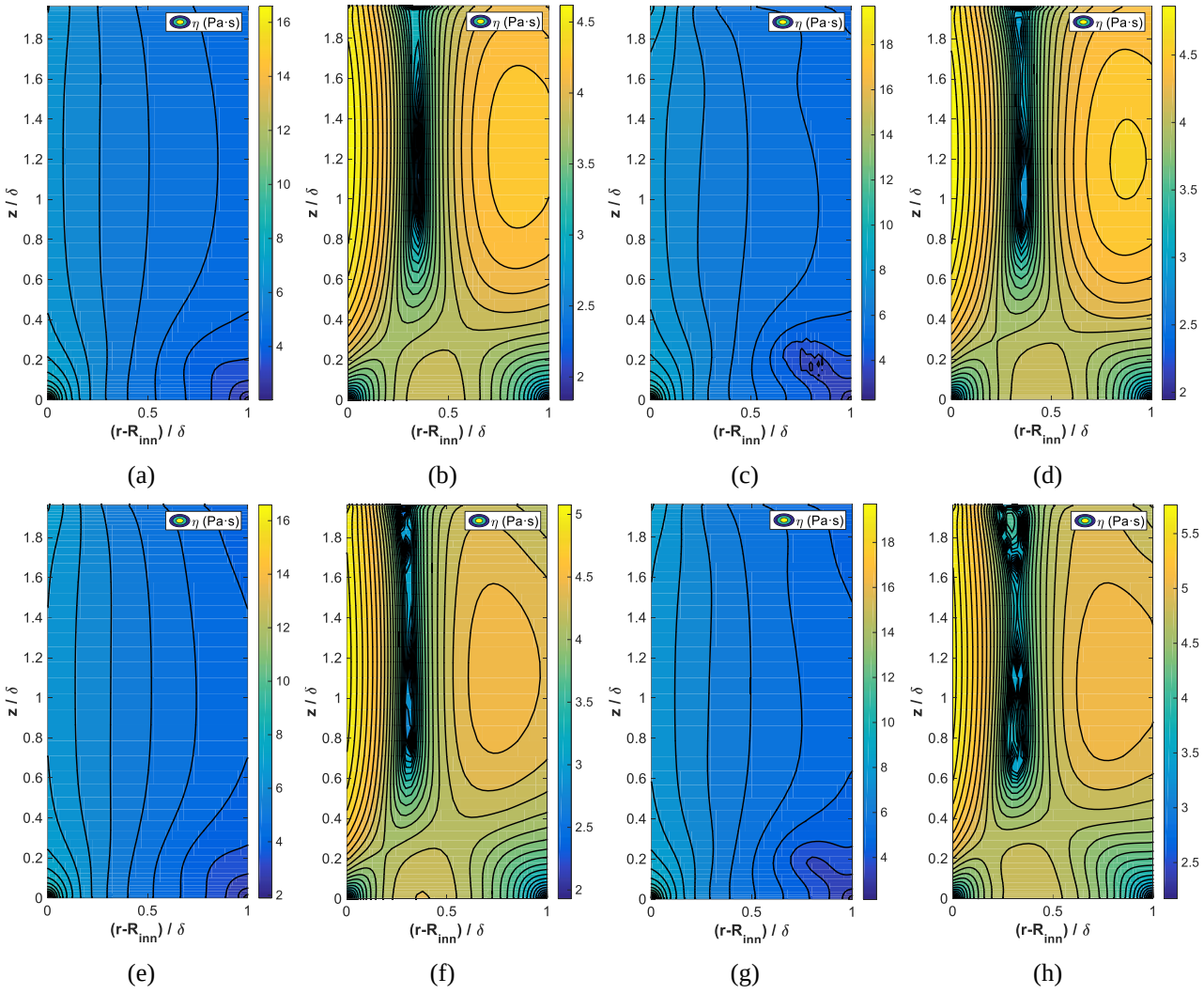

Figure 7. Apparent viscosity fields observed in different positions and at different time instants of the periodic simulations using Mix 1 as working fluid: for Test 1 (a) 2.0 s; (b) 2.96 s; for Test 2 (c) 2.0 s; (d) 2.96 s, for Test 3 (e) 1.0 s; (f) 1.48 s; for Test 4 (g) 1.0 s (h) 1.48s.

5. CONCLUSIONS

The numerical scheme was able to predict the behavior of different water-fabric mixtures when exposed to periodic simulations, which attempted to simulate a vertical-axis washing machine. Despite not being capable to predict the correct torque value at the peaks where the inner cylinder presents an abrupt change of velocity, it was capable to predict a similar torque value for the maximum velocity periods when compared to the experimental database. Moreover, the assumption to model the water-fabric mixture as a non-Newtonian fluid, by means of the so-called Generalized Newtonian fluid approach with yield stress (Herschel-Bulkley model), was able to predict the apparent viscosity of the fluid in the entire three-dimensional physical domain of the washing machine, thus pointing out the regions where a higher resistance is observed and where the mixture flows with less resistance. Such an analysis can be applied by washing machine design engineers to maximize the mechanical efficiency of the cloth washing process.

A qualitatively and quantitively analysis of the apparent viscosity field was presented for the sake of comparison of different numerical tests: (a) with and without a rotating basis; (b) different working fluids; and (c) different tests. It was observed that the presence of a rotating basis enhances the applied torque at the fluid and also the mixing of the mixture

within the concentric cylinders over time, which is a desirable effect to maximize the mechanical efficiency of the washing process, for example. The different mixtures behavior come from the bulk of fabric used to characterize the fabric-water mixtures (Mix 1 and Mix 2). As the fluid is characterized as dilatant (behavior index over-unity), it is expected that the apparent viscosity is higher at the points with maximum torque. Finally, it was observed that for the same fluid, the tests present similar apparent viscosity fields at the end of the time-on and time-off periods, where the main difference comes from the maximum imposed angular velocity for different testes. Nevertheless, there was observed a peak of torque values right after the acceleration and deceleration periods, which may enhance the washing efficiency, thus denoting that shorter cycles may represent an efficiency enhance in the process.

6. ACKNOWLEDGEMENTS

This study was carried out at under the auspices of the Brazilian government funding agencies and CAPES PDSE (Grant no. 99999.010196/2014-05) and CNPq (Grant no. 470986/2012-3). Dr. F. R. Loyola duly acknowledges Dr. Shinji Tamano for hosting him for one year at the Nagoya Institute of Technology, during which improvements in the CFD code were performed.

7. REFERENCES

Ahlberg JH, Nilson EN, Walsh JL (1967) The Theory of Splines and Their Applications: A Series of Monographs and Textbooks. Academic Press, New York

Campos LG, Hermes CJL (2016) Experimental evaluation and transient simulation of detergent transport in household vertical axis washing machines. Chemical Engineering Research and Design 109:720-729

Donnelly, RJ (1991) Taylor-Couette Flow: The Early Day. Physics Today 44:32-39

Loyola FR, e Silva Jr WL, Campos LG, Hermes CJL (2018). Rheometric assessment and numerical simulation of steady-state and periodic flows of fabric-water mixtures in household top-load washing machines. Chemical Engineering Research and Design, 137, 273-290.

Maliska CR, Raithby GD (1983) Calculating three-dimensional fluid flows using nonorthogonal grids. Proc. 3rd Int. Conf. On Numerical Methods in Laminar and Turbulent Flows, Seattle: 656-666

Mitsoulis E (2007) Flows of viscoplastic materials: models and computations. Rheology Reviews:135-178

Papanastasiou TC (1987) Flows of Materials with Yield. Journal of Rheology 31:385-404

Patankar S (1980) Numerical Heat Transfer and Fluid Flow. Hemisphere Publishing Co., New York

Van den Brekel LDM (1987) Hydrodynamics and mass transfer in domestic drum-type washing machines. Doctorate Dissertation, TU Delft

Van der Vorst HA (1992) Bi-CGSTAB: A Fast and Smoothly Converging Variant of Bi-CG for the Solution of Nonsymmetric Linear Systems. SIAM Journal on Scientific and Statistical Computing 13:631–644.

8. RESPONSIBILITY NOTICE

The authors are the only responsible for the printed material included in this paper.